Indian Journal of Natural Products and Resources
Vol. 16(3), September 2025, pp. 353-373
DOI: 10.56042/ijnpr.v16i3.16273

Trispectroscopy UV-VIS, FT-IR, and GC-MS profiling and anticancer potentials of *Senna italica* (Mill.) targeted caspase-3: Molecular docking and *in vitro* insights

Fouzi S. Aboud[1,2*], Majed A. Al-Shaeri[1,3], Ali T. Zari[1,4,5], Ehab M. M. Ali[6,7], Naif A. Almalki[6,8] and Naser A. Alkenani[1,3]

[1]Department of Biological Sciences,[3] Environmental Protection and Sustainability Research Group, [6]Department of Biochemistry, Faculty of Science, King Abdulaziz University, Jeddah 21589, Saudi Arabia

[2]Department of Anatomy, Histology and Embryology, Faculty of Medicine, University of Tripoli 13932, Tripoli, Libya

[4]Centre of Excellence in Bionanoscience,[5] Princess Dr. Najla Bint Saud Al-Saud Centre for Excellence Research in Biotechnology, King Abdulaziz University, Jeddah 21589, Saudi Arabia

[7]Department of Chemistry, Faculty of Science, Tanta University, Tanta 3152, Egypt

[8]Experimental Biochemistry Unit, King Fahd Medical Research Centre, King Abdulaziz University, Jeddah 21589, Saudi Arabia

Received 08 January 2025; revised received 15 July 2025; accepted 28 July 2025

Distant metastases account for the majority of breast cancer–related deaths. The median survival time for women with breast cancer (BC) metastasized to the liver is less than three years. In this study, leaves of *Senna italica* (Mill.) were macerated in 80% ethanol and concentrated using a precision economy incubator. Tri-spectroscopic analytical techniques (UV-VIS, FT-IR, and GC-MS) were employed to characterize the chemical structures of the extracted compounds. Molecular docking, molecular dynamics simulations, and pharmacokinetic analyses were performed to evaluate the binding affinity, stability, and solubility of selected compounds targeting caspase-3. Normal human skin fibroblasts (HSF) and BC cell lines (MCF-7, T47D, MDA-MB-231), along with the liver cancer (LC) cell line (HePG2), were cultured for 24 and 48 hours to assess acute toxicity, antiproliferative effects, and caspase-3 activation by the extracts. Pharmacokinetic profiling of compound CID-624232 (Benzo-furor-pyrimidinylfluoro-phenyl-amine) indicated favourable solubility, stable binding, and strong interactions with the target protein. Antiproliferative assays demonstrated that the extracts exhibited no cytotoxicity toward normal HSF cells, with an IC_{50} value of 869.6±5.04 µg/mL. In contrast, a significant inhibition of cell proliferation was observed in LC HePG2 cells, with IC_{50} values of 145.89±2.76 µg/mL and 98.04±2.23 µg/mL after 24 and 48 hours of treatment, respectively, accompanied by increased caspase-3 levels. These findings suggest that benzo-phenyl-amine compounds isolated from *S. italica* may inhibit the proliferation of breast and liver cancer cells through activation of the pro-apoptotic protein caspase-3.

Keywords: Breast and liver cancer cells, Caspase-3, Cytotoxicity, *In silico* modelling, *Senna* species, Threefold spectroscopic analysis

IPC code; Int. cl. (2021.01)– A61K 36/00, A61K 36/48, A61K 127/00, A61P 35/00

Introduction

Gloabally, cancer continues to be a major cause of death, representing a serious challenge to public health. In 2020, an estimated 20 million new cases were identified, with close to 10 million deaths attributed to the disease across all ages and genders[1]. In women, breast carcinomas (BC) stands as the most frequently diagnosed form of cancer, accounted for over two million new cases and more than 500,000 deaths. According to global projections, the annual incidence of BC is expected to surpass 3 million cases, with over one million deaths due to population growth and aging. Triple-negative receptor (ER^-, PR^-, $HER2^-$) is the most aggressive BC subtype, characterized by a poor prognosis largely resulting from tumor heterogeneity and resistance to therapy[2].

Liver cancer (LC), including hepatocellular carcinoma (HCC), ranks among the five most fatal cancers and is especially prevalent in developing nations. Risk factors such as chronic liver infections, fatty liver disease, and diabetes significantly contribute to HCC development. Surgical resection remains the most viable treatment option in early stages; however, the prognosis is typically poor[3]. Additionally, distant metastasis is a major contributor

*Correspondent author
Email: fmiftah@stu.kau.edu.sa

to BC-related deaths. For instance, the median survival of women with breast cancer liver metastasis is approximately 2–3 years. Although all subtypes of BC can metastasize to the liver, HER2-positive tumours show a higher tendency to do so[4].

In the search for novel, effective anticancer therapies, natural products derived from medicinal plants have gained considerable attention. Saudi Arabia is home to a rich diversity of flora, with the Saudi Pharmacopeia documenting 96 medicinal plant species across 47 families. Many of these are traditionally used by locals for therapeutic purposes, particularly the leaves and aerial parts[5]. One such promising genus is *Senna*, which includes around 350 species of trees, shrubs, and subshrubs in the legume family[6]. Senna italica (Mill.), a perennial leguminous herb belonging to the Fabaceae family, is commonly found throughout tropical and subtropical regions, including Saudi Arabia[7]. Its phytochemical profile includes pentacyclic triterpenes, alkaloids, piperidines, flavonoids, tannins, anthocyanins, catechins, leucoanthocyanins, sennosides, and anthraquinones, which have demonstrated various therapeutic potentials[8].

Many plant-derived compounds are hydrophobic in nature, which may limit their solubility and bioavailability. To address this issue, green extraction methods using ionic liquids such as ethanol, methanol, ethyl ether, and chloroformare employed to isolate both hydrophilic and hydrophobic phytochemicals from plant materials[9]. Analytical techniques like gas chromatography and infrared spectroscopy aid in the purification and structural identification of these compounds[10]. Furthermore, modern computational tools have transformed early drug discovery by enabling the prediction of biological activity and pharmacokinetic behaviour. Molecular docking, for example, is used to model interactions between small molecules and target receptors, offering insights into potential mechanisms of action. In parallel, pharmacokinetic prediction software helps estimate absorption, distribution, metabolism, excretion, and toxicity profiles, thus saving time and resources in drug development[11].

Despite previous studies detecting various phytoconstituents in aerial parts of each *S. italica* (Mill.) extracts[12,13], they may differ depending on growth environment, climate conditions, soil compositions, and structure. Radwa Mount was selected for its distinctive biodiversity to collect plant samples. It consists of many mountains in one mount in the Yanbu Al Nakhil Mountains. Different floristic composition, numerous native and endemic plant species are grown[14]. Therefore, we employed a comprehensive biomolecular approach to assess the solubility, stability, and binding affinity of compounds derived from *S. italica* (Mill.) leaves toward caspase-3, a key protein involved in apoptosis. To the best of our knowledge, this study is among the first to integrate biochemical, molecular, and *in vitro* techniques to evaluate *S. italica*-based candidates targeting caspase-3 for potential cancer therapy.

Materials and Methods

Chemicals and reagents

The materials used in this study included ethanol (Sigma-Aldrich®), Dulbecco's Modified Eagle Medium (DMEM) (Hyclone®), phosphate-buffered saline (PBS) (Hyclone®), fetal bovine serum (FBS) (Hyclone®), trypsin-EDTA (Hyclone®), dimethyl sulfoxide (DMSO) (Sigma-Aldrich®), doxorubicin (DOX) (SWISS PARENTERALS LTD®), the MTT assay kit (Sigma-Aldrich®), and the Caspase-Glo 3 assay kit (Promega®).

Equipment and software

The equipment employed in the experiments included Milli-Q water (MILLIPORE SAS®), a digital orbital shaker (DAIH-SCIENTIFIC®), a precision economy incubator (Thermo-Fisher Scientific®), an ultraviolet-visible spectrophotometer (Bibby Scientific®), Fourier-transform infrared spectroscopy (Thermo-Fisher Scientific®), a gas chromatograph–mass spectrometer (Agilent®), a microplate reader (Agilent®), and an inverted microscope (LABOMED®). The software used for molecular dynamics and computational analyses comprised the Research Collaboratory for Structural Bioinformatics Protein Data Bank (RCSB-PDB), BIOVIA Discovery Studio, PyMOL 2.5.0, CASTp, PyRx Virtual Screening Tools, PubChem, Microsoft Excel 2016, GROningen MAchine for Chemical Simulations (GROMACS), the Chemistry at Harvard Macromolecular Mechanics (CHARMM) General Force Field (CGenFF) server, and DiffDock.

Plant material

Fresh leaves of *S. italica* were collected in January 2024, from Yanbu governorate in the middle of Radwa Mountain in the western region of Al-Madinah Al-Munawwara, KSA. The samples were classified and authenticated by a plant taxonomist at the Department of Biology, KAU, with sample voucher

SiM18461. The leaves were air-dried in the shade at ambient room temperature for a period of three weeks. The dried leaves were crushed using a mechanical grinder until a soft powder was obtained and kept in an airtight container in a dry place for further experiments.

Extract preparation

Dried powdered *S. italica* leaves (25 g) were extracted by maceration with 250 mL ethanol 80% (Sigma-Aldrich®) for 72 hours at room temperature with a digital orbital shaker (DAIH-SCIENTIFIC®). The extracted solution was filtered with Whatman No.1 filter paper, and the filtrate was evaporated in the dark using a precision economy incubator (Thermo-Fisher Scientific®) at 40°C for 2 hours to obtain a dry extract.

Ultraviolet-visible (UV-VIS) spectrophotometer

An ultraviolet-visible (UV-VIS) spectrophotometer (Bibby Scientific®) was used to identify the main band patterns. The *S. italica* leaf extract was examined under UV-VIS light at wavelengths ranging from 200 to 800 nm using the same solvent at a 1:10 ratio.

Fourier-transform infrared spectroscopy (FT-IR)

To identify the main functional groups in the ethanolic extraction of *S. italica*, a small amount of the extract was placed ona sample holder. Absorbance and transparent analysis were then performed using Fourier-transfer infrared (FT-IR) spectroscopy (Thermo-Fisher Scientific®), which was scanned from 4000 to 500 cm^{-1}.

Gas chromatograph mass spectroscopy (GC-MS)

Bioactive compounds of *S. italica* were isolated using capillary column gas chromatograph mass spectrometer (GC-MS) (Agilent®). The sample was injected into the spectrometer in split mode and at a 300°C injection port temperature setting. The helium flow rate was 1.61 mL/min at 280°C. The temperature increased by approximately 10°C per minute, starting at 50°C in the first minute, and eventually reaching 300°C. The scan mode was used for a total of 32 minutes, covering a range of 40 to 500 m/z range. The molecules were then identified using the NIST~98 mass spectral database.

Molecular docking (MD) study

Protein preparation

For molecular docking and simulation process involving caspase-3, 1GFW was selected as a common reference structure, as well as it's well-resolved and has the active site clearly defined. The three-dimensional structure of caspase-3 (1GFW) was downloaded from the Research Collaboratory for Structural Bioinformatics-Protein Data Bank (RCSB-PDB) in PDB format (three-dimensional structure). After that, the protein was accoutred and defected by removing side chains, water, and ligand molecules using BIOVIA Discovery Studio and PyMOL 2.5.0 software, as shown in Fig. 1.

Ligand preparation

The chemical structures of selected isolated compounds from *S. italica*: Hydroxyphenyl-dihydro-benzo-quinazoline (CID: 631675); Chloro-methyl-pyrazole with trifluoromethyl phenyl oxymethanone (CID: 9603144); Benzene sulfonamide-amino-1naphthhalenyl (CID: 91722819); and Benzo-furor-pyrimidinylfluoro-phenyl-amine (CID: 624232), were downloaded from PubChem (*https://www.pubchem.ncbi. nlm.nih.gov/*). These structures were then analyzed using AutoDockVina and PyRx virtual screening software, to determine the ligands with the highest binding affinity.

Generating of receptor grid

A grid was created in Glide with a default Van der Waals radius scaling factor of 1.0 and a charge cutoff of 0.25. The minimized structure was then exposed to the OPLS_2005 force field. The ligand active site was surrounded by a cubic box, fitted to 14 × 14 × 14 $Å^3$ for docking the four selected ligands with the 1GFW protein one by one.

Computational pharmacokinetics

ADMET, which categorizes pharmaceuticals based on absorption, distribution, metabolism, excretion, and toxicity, provides the best description of the relationship between medication dosages and their concentrations over time. When selecting a chemical

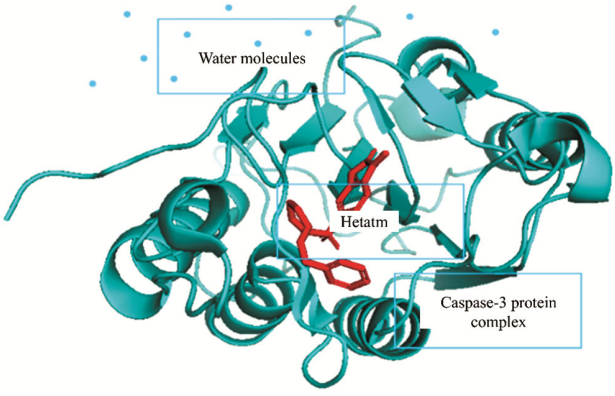

Fig. 1 — Molecular 3D structure of caspase-3 (1GFW) protein from *Homo sapiens*.

for potential therapy, we first examine its analogs by carefully choosing compounds that can affect both *in vivo* and *in vitro* experimental outcomes. Swiss-ADME is an online program available at *http://www.swissadme.ch/index.php* that assesses a compound's solubility, bioavailability, and toxicity to identify potentially beneficial options. Furthermore, the safety profiles of the compounds were evaluated using computer-aided design and drafting (CADD).

Molecular dynamics (MD) simulation study

Molecular dynamics (MD) simulations were performed using GROningen MAchine for Chemical Simulations (GROMACS). The crystal structure of caspase-3 (RCSB-PDB ID: 1GFW) and ligand parameters were generated using the Chemistry at Harvard Macromolecular Mechanics (CHARMM) General Force Field (GenFF) server, which provided topology files for all compounds. The protein was modeled with the CHARMM36 force field, while ligands were parameterized using CGenFF. The system was solvated in a cubic box containing transferable intermolecular potential three-point water molecules, and counterions were added to neutralize the overall charge. Energy minimization was carried out using the steepest descent algorithm to remove steric clashes and unfavourable contacts, and continued until the maximum atomic force was below 1000 kJ/mol/nm. The system was then equilibrated in two phases: first, a 100 picoseconds under conditions of constant number of particles, constant volume, and constant temperature at 300 K using a modified Berendsen thermostat equilibration at 300 K using a modified Berendsen thermostat, followed by the second phase consisted of a 100 picoseconds equilibration under conditions of constant number of particles, constant pressure, and constant temperature at 1 bar using the Parrinello-Rahman barostat, with the heavy atoms of the protein and ligands constrained during both equilibration steps. Bond lengths were constrained using the Linear Constraint Solver algorithm with a two femtosecond time step. The Verlet cutoff scheme was applied for neighbor searching with a 1.2 nm cutoff for non-bonded interactions, and long-range electrostatics were treated using the Particle Mesh Ewald method Abraham *et al.*[15].

***In vitro* study**

Preparation of the stock solution

The crude extract obtained from *S. italica* was diluted to 10 mg in 1 mL of Dimethyl Sulphoxide (DMSO). A stock solution of doxorubicin (DOX) was prepared by adding 2.5 µL of 20 mg to 2 mL of media to achieve a 50 µg/mL concentration.

Cell culture sub-culture preparation

Normal human skin fibroblasts (HSF), along with BC cancer cell lines MCF-7, T47D, and MDA-MB-231, and the LC cell line HePG2, were obtained from the King Fahd Medical Research Center in Jeddah, Saudi Arabia. All cell lines were cultured separately in sterile T25 flasks containing complete Dulbecco's Modified Eagle Medium (DMEM) supplemented with 10% fetal bovine serum (FBS) and maintained in a humidified incubator with a 5% CO_2 at 37°C. Once the cells reached approximately 90% confluence, cancer cells were detached by briefly incubating with 1.5 mL of 0.25% trypsin at 37°C for 5 minutes. Trypsin activity was then neutralized by adding culture medium, and the cells were collected by centrifugation at 1500 rpm for five minutes, washed twice with phosphate-buffered saline (PBS), and resuspended in 5 mL of fresh medium. Cell counts were determined using a hemocytometer with the trypan blue exclusion method. Cells were subcultured every three to four days by first washing the monolayers with PBS and then performing a brief trypsinization. Only cells in the exponential growth phase were used for all experimental assays.

Antiproliferative assay

The MTT assay was employed to evaluate the cytotoxic effects of DOX and the ethanolic extract of *S. italica* on normal HSF cells, BC (MCF-7, T47D, and MDA-MB-231), and LC HePG2 cells. Cells were seeded at a density of 9×10^3 cells per well and incubated overnight. The culture medium was then carefully removed and replaced with 100 µL of fresh medium containing varying concentrations of DOX (3.125–50 µg/mL) or *S. italica* crude extract (50–800 µg/mL). After treatment, 10 µL of MTT solution was added to each well, and the plates were incubated for 3 hours. The resulting formazan crystals formed by metabolically active cells were dissolved with 100 µL of DMSO, followed by gentle shaking for 10 minutes to ensure complete solubilization. Cell viability was subsequently determined by measuring the absorbance at 490 nm using a microplate reader, and the results were expressed relative to untreated control cells.

Microscopic examination

After 24 and 48 hours of treatment, the morphology of the cultured BC and LC cells was

observed using a LABOMED® inverted microscope. Images were captured to assess the effects of the treatments on cell morphology.

Calculation of selectivity index

The selectivity index (SI) is defined as the ratio between the toxic concentration of a sample and its effective bioactive concentration. An ideal therapeutic agent exhibits low toxicity toward normal cells while maintaining high efficacy against target malignant cells. In studies involving medicinal plants or isolated compounds, SI values are critical for evaluating safety and effectiveness. The SI was calculated for all tested cell lines by dividing the IC_{50} value of normal cells by that of cancer cells. Typically, the SI values observed ranged from 1.96 to 51.3[16].

$$SI = \frac{IC_{50}^{Non-Malignant\ cells}}{IC_{50}^{Maligant\ cells}}$$

Caspase-3 activity assay

Caspase activity was evaluated using a luminescent Caspase-Glo® 3 assay kit (Promega®). LC HePG2 cells were first seeded and allowed to grow, then exposed to different concentrations of DOX (1.5, 3, and 6 µg/mL) and *S. italica* extract (50, 100, and 200 µg/mL). The Caspase-Glo 3 reagent was added directly to the wells without removing the culture medium, and the plates were incubated at room temperature for 3 hours. Luminescence was subsequently recorded using a microplate reader (Agilent®).

Statistical analysis

Statistical analyses were conducted using GraphPad Prism 8 and Microsoft Excel 2016. Experimental data are expressed as mean ± standard deviation from three replicates. A P-value of less than 0.05 was considered statistically significant. Differences between untreated and treated groups were assessed using one-way ANOVA followed by Tukey's multiple comparison test. A P-value below 0.001 was indicated with asterisks (***) and (**).

Results

Phytochemical profiles of *S. italica* extract

The UV-VIS spectra analysis of *S. italica* extract showed different band patterns in the two clusters. Cluster I in the 200-280 nm range can be related to the electronic transition of double-bond electrons in olefinic compounds. Cluster II in the wavelength range from 290 to 50 nm is attributed to the electronic transition from non-bonding electrons in carbonyl (C=O) and carboxyl (O=C-OH) groups (Table 1 and Fig. 2a).

The FT-IR peak intensities, positions, and corresponding functional groups were identified based on the relative ratio of each peak in the infrared spectra. The FT-IR spectra displayed a broad absorption band in the range of approximately 3310–3370 cm^{-1}, corresponding to O–H stretching vibrations typically found in phenolic and/or alcohol groups. Two peaks were observed between roughly 2860 and 2940 cm^{-1}, which are characteristic of C–H stretching vibrations in methyl and methylene groups. Peaks in the ranges of about 1710–1720 cm^{-1} and 1610–1650 cm^{-1} were attributed to C=O and C=C double-bond stretching vibrations, respectively. The band around 1420–1450 cm^{-1} was assigned to C–H bending vibrations in saccharide groups. Absorption peaks between approximately 1360–1370 cm^{-1} and 1220–1230 cm^{-1} were associated with C–H bending vibrations of ester groups and C–O stretching vibrations in ester and/or glycoside functional groups. Finally, the absorption band in the range of 1050–1060 cm^{-1} indicated the presence of alcohols and saccharides (Table 2 and Fig. 2b).

Additionally, 15 intriguing bioactive compounds were identified in theethanolic extract of *S. italica* leaves through GC-MS. The chemical formula, retention time, and concentration were determined throughout the chromatographic period (Table 3 and Fig. 2c).

MD analysis

Active sites searching

The active protein binding sites were identified using the PyMOL server. The targeted receptor (1GFW) exhibited binding sites mainly at the positions of ARG 207, CYS 163, GLU 122, SER 120, SER 205, TYR 204, MET 61, HIS 121, PHE 250, and TRP 206 at three short distances 2.6 Å, 3.0 Å, and 3.3 Å, Table 4 and Fig. 3.

Table 1 — UV-VIS spectra peak characterization of *S. italica* (Mill.)

Sample	Wavelength (nm)	Absorbance	Functional groups
S. Italica (Mill.)	265	0.57	Double bonds (olefinic and aromatic compounds)
	352	0.36	Non-bonding electron in (C=O) and (O=C-OH) groups

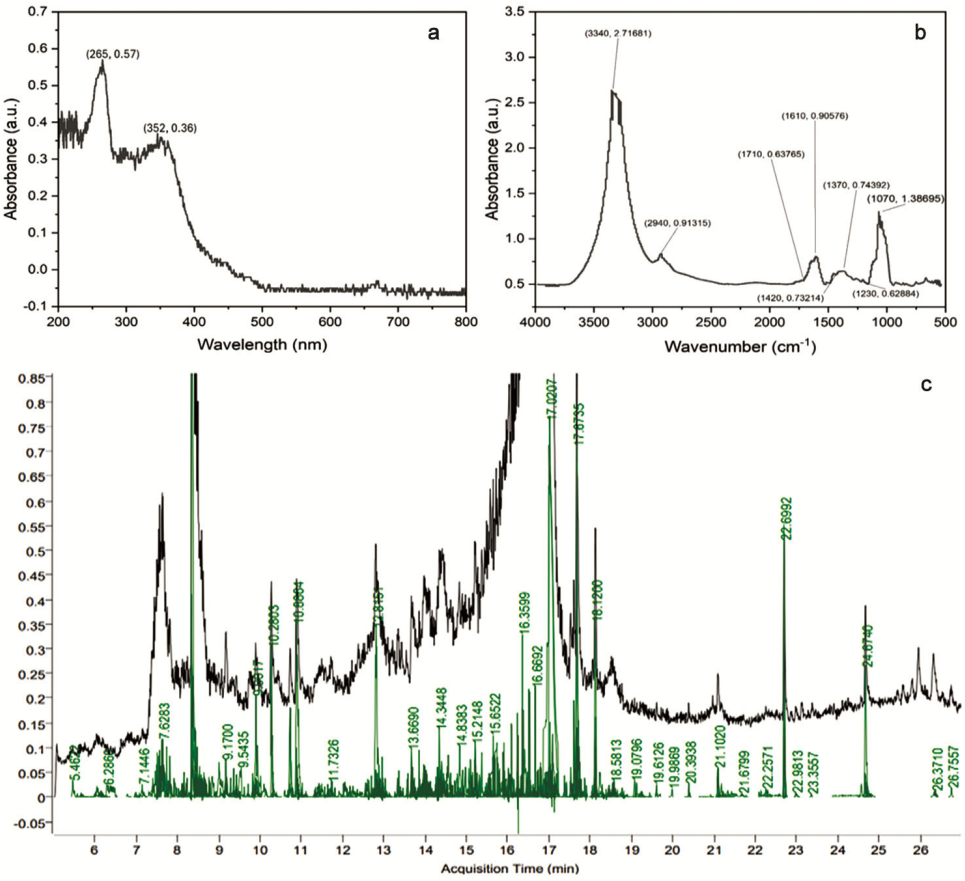

Fig. 2 — Spectroscopic analysis of *S. italica* (Mill.) extract using three techniques: a) UV–VIS, b) FT–IR, and c) GC–MS, showing the main detectable bioactive constituents.

Table 2 — FT-IR spectra peak characterization of *S. italica* (Mill.)

Sample	Wave number (cm^{-1})	Intensity	Bond responsible
S. Italica (Mill.)	3340	2.71	ν:O-H (Phenolic, Alcohol)
	2940	0.91	ν:C-H (Methyl & Methylene)
	1710	0.63	ν:C=O (Ester)
	1610	0.91	ν:C=C (Aromatic rings); δ: N-H (Amine)
	1420	0.73	δ:C-H (Saccharides)
	1370	0.74	δ:C-H (Ester)
	1230	0.63	ν:C-O (Ester, glycoside)
	1050	1.38	ν:C-O (Alcohol,acid, Saccharides)

Table 3 — GC-MS analysis of ethanolic extract of *S. italica* (Mill.)

Peak	Compound retention time	Compounds	Compound formula	Compound area	Compound (%)
1	6.0466	Benzo-furo-pyrimidinylfluoro-phenyl-amine	$C_{16}H_{10}FN_3O$	7279833.8	66.2
2	6.9946	Phenylmethylazetidinecarbothioic acid derivative	$C_{17}H_{17}NOS$	1932850.8	51.4
3	8.1105	Hydroxyphenyl-dihydrobenzoquinazoline	$C_{24}H_{18}N_2O$	842334.3	51.1
4	9.1950	Dimethyl bis(phenyl) phthalamide	$C_{22}H_{20}N_2O_2$	6572644.1	61.1
5	9.9614	Chloro-methyl-pyrazole-trifluoromethyl phenyl oxymethanone	$C_{13}H_9ClF_3N_3O_2$	4803982.1	52.9

(*Contd.*)

Table 3 — GC-MS analysis of ethanolic extract of *S. italica* (Mill.) (*Contd.*)

Peak	Compound retention time	Compounds	Compound formula	Compound area	Compound (%)
6	10.3977	Dichloro-dinitrophenyl hydrazone	$C_{13}H_9ClN_4O_5$	2595945.5	58.1
7	11.6997	Amino-pyrimidinyl benzoic acid	$C_{11}H_9N_3O_3$	4538203.2	52.4
8	12.1865	Difluorobenzoyl phenyl isoxazolone	$C_{16}H_9F_2NO_3$	3564082.5	69.9
9	13.6521	Catechol derivative methylbenzoyl and trifluoromethylcinnamoyl groups	$C_{24}H_{17}F_3O_4$	981899.3	51.4
10	15.9449	Chloro-fluoro-benzoic acid nitrophenyl ester	$C_{13}H_7ClFNO_4$	1268471.5	52.4
11	16.2367	Difluoro-methylbenzoic acid tetrachloro-phenyl ester	$C_{14}H_6Cl_4F_2O_2$	1612968.8	69.9
12	16.8219	Benzyl-methoxyphenyl-dioxoaziridinopyrrolidine	$C_{18}H_{16}N_2O_3$	3165440.6	58.9
13	16.8313	Benzene sulfonamide-amino-naphthalene	$C_{17}H_{16}N_2O_2S$	4078127.2	53.5
14	21.3953	Methoxyphenyl methyl-trifluoromethylpyrazolecarboxamide	$C_{13}H_{12}F_3N_3O_2$	930459.8	50.1
15	23.3557	Dimethoxybenzaldehydehydrazone with methoxybenzoyl	$C_{17}H_{18}N_2O_4$	775557.8	52.7

Table 4 — Active site prediction of targeted protein caspase-3

Protein	Volume (SA)	Area (SA)	Resolution	Total AA residue in chain A	AA residues at predictive active site
Caspase-3	64.032	82.180	1.75	147	29

SA: surface area; AA: amino acids

Table 5 — Molecular docking scores of selected compounds from the *S. italica* (Mill.)

S. No.	Chemical name	PubChem ID	MF	MW	BA (Kcal/mol)
1	Hydroxyphenyl-dihydrobenzoquinazoline	CID 631675	$C_{24}H_{18}N_2O$	350.4 g/mol	-8.3
2	Chloro-methyl-pyrazole- trifluoromethyl phenyl oxymethanone	CID 9603144	$C_{13}H_9ClF_3N_3O_2$	331.68 g/mol	-7.5
3	Benzene sulfonamide-amino-1-naphthalenyl	CID 91722819	$C_{17}H_{16}N_2O_2S$	312.4 g/mol	-7.5
4	Benzo-furo-pyrimidinylfluoro-phenyl-amine	CID 624232	$C_{16}H_{10}FN_3O$	279.27 g/mol	-7.4

CID: Compound ID; MF: Molecular Formula; MW: Molecular Weight; BA: Binding Affinity

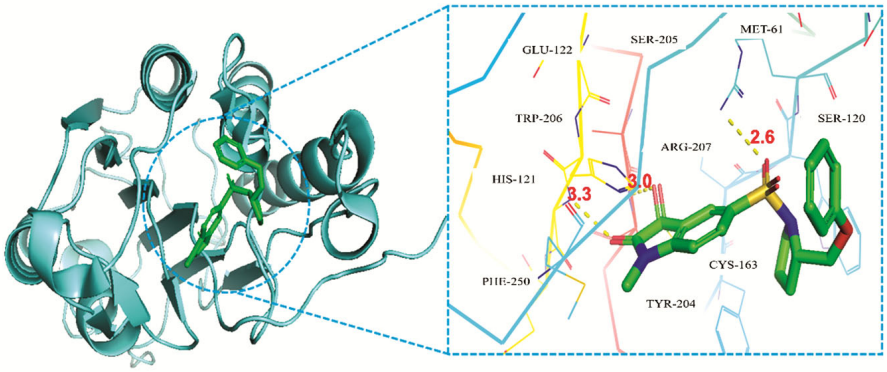

Fig. 3 — Caspase-3 (IGFW) protein active pocket showing the amino acid residue.

MD between four selected compounds and receptor

The total of 15 bioactive compounds from *S. italica* were docked with the 1GFW receptor using PyRx tools and AutoDockVina, resulting in binding affinity values ranging from -3.1 to -8.3, and four compounds were selected for further molecular analysis because of their high binding scores as summarized in Table 5 and illustrated as CID-631675 (Fig. 4a), CID-9603144 (Fig. 4b), CID-91722819 (Fig. 4c), and CID-624232 (Fig. 4d).

Hydrogen bonding and hydrophobic interactions play a key role in the binding affinity between compounds and their target receptor. In our validation, compound CID-631675 formed hydrogen

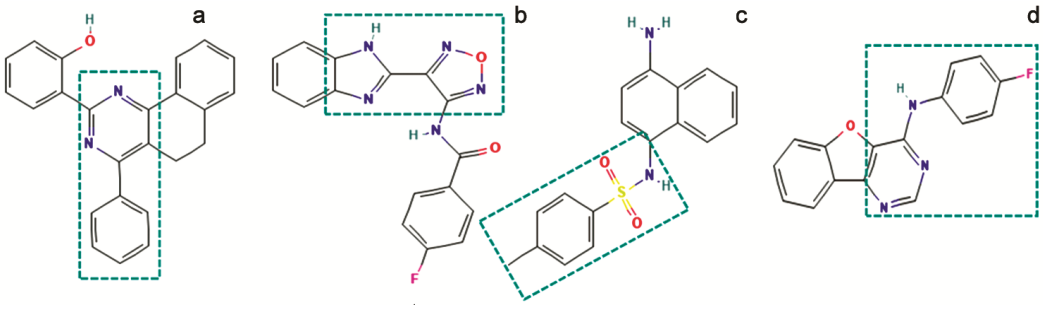

Fig. 4(a-d) — The chemical structure of four selected compounds: a) CID-631675, b) CID-9603144, c) CID-91722819, and d) CID-624232 from *S. italica* (Mill.).

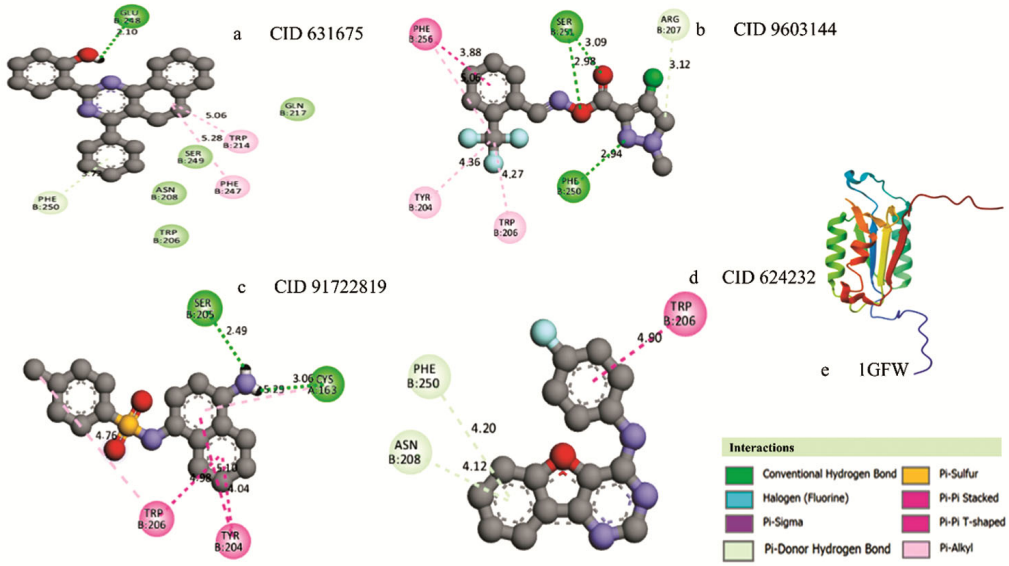

Fig. 5 — 2D interactions of selected compounds from the ethanolic extract of *S. italica* (Mill.) with caspase-3 (PDB ID: 1FGW): a) CID 631675: Hydroxyphenyl-dihydrobenzoquinazoline, b) CID 9603144: Chloro-methyl-pyrazole- trifluoromethyl phenyl oxymethanone, c) CID 9172219: Benzene sulfonamide-amino-1-naphthalenyl, d) CID 624232: Benzo-furo-pyrimidinylfluoro-phenyl-amine, and e) caspase-3 protein structure (1GFW).

bonds with GLU248 and PHE250 at distances of 2.10 and 3.72 Å, respectively, and hydrophobic interactions with TRP214 and PHE247 at 5.06 and 5.28 Å (Fig. 5a). For compound CID-9603144, hydrogen bonds were observed with SER251 (3.09 and 2.98 Å) and PHE250 (2.94 Å), while multiple hydrophobic contacts were detected with PHE256, TYR204, and TRP206 at distances of 3.88, 4.36, and 4.27 Å, respectively (Fig. 5b). Compound CID-91722819 exhibited hydrogen bonds with SER205 and CYS163 at 2.49 and 3.06 Å, along with hydrophobic interactions at TRP206 and TYR204 (4.98 and 4.04 Å) (Fig. 5c). Finally, CID-624232 displayed hydrogen bonds with PHE250 and ASN208 and hydrophobic contacts at TRP206, all at distances around 4.0 Å (Fig. 5d), indicating stable interactions with IGFW (Fig. 5e).

ADMTE properties of extracted compounds

Computational Molecular docking methods were used to screen compounds from a pure ethanolic extract of *S. italica* based on binding affinity. The extracted bioactive compounds exhibited strong binding affinity, which was attributed to the formation of numerous hydrogen bonds and hydrophobic interactions between the ligands and the target receptors. However, according to Lipinski's rule of five[17], which limits the molecular weight (MW) to < 500 g/mol, the number of hydrogen bond donors (HBD) should be < 5, while hydrogen bond acceptors (HBA) should be < 10. All active compounds of *S. italica* were detected within the recommended range.

According to the Swiss-ADMET, compound 12 of *S. italica* showed a log P value of 6.81, exceeding

the required range (-2.0 – 6.5). Log-P reflects the lipophilicity of a compound. The solubility of substances that directly affect absorption was measured using Log-S. Most of the studied compounds demonstrated moderate-to-well-qualified solubility. However, compounds 2,4,5,8,10, and 12 appeared to be poorly soluble. The bioactive compounds 2,3,4,5,6,8,10, and 13 of *S. italica* demonstrated the ability to crossthe blood-brain barrier (BBB), whereas compounds 1, 7, 9, 11, 12, 14, and 15 are unable to cross the BBB. Additionally, all the compounds of plant extracts were good candidates for gastrointestinal absorption, except for compounds 10 and 12, which showed lower absorption capacities. Moreover, none of thebioactive compounds of the studied medicinal plants showed any indications of cytotoxicity (Table 6).

MD simulation analysis

Comparing the four protein–ligand complexes, the root mean square deviation **(**RMSD) values for compounds CID-631675 and CID-9603144 were higher after 20 ns, indicating more structural changes in the protein. Compound CID-91722819 showed stable RMSD values with more fluctuations than compound CID-624232, which had the most stable RMSD values after 40 ns, suggesting that it underwent the least structural changes in the protein (Fig. 6a). The root mean square fluctuation (RMSF) analysis of CID-631675 and CID-624232 compounds showed lower RMSF values in the central residues, indicating stability. In contrast, compound CID-9603144 exhibited higher values in specific regions, indicating increased flexibility, while compound CID-91722819 showed the highest fluctuations at the N- and C-terminal residues, suggesting enhanced flexibility at the protein termini (Fig. 6b).

The radius of gyration (Rg) of the protein–ligand complexes for the selected compounds showed initial fluctuations, reflecting early adjustments in the protein structure, and generally stabilized over time with minor variations. For compound CID-631675, slightly lower Rg values were observed during the later stages of the simulation. In contrast, CID-9603144 exhibited higher fluctuations, reaching up to 1.8 nm, suggesting greater structural expansion and flexibility. Compound CID-91722819 displayed moderate Rg fluctuations between approximately 1.3 and 1.6 nm, indicating moderate stability and compactness, while CID-624232 maintained consistent Rg values around 1.4 to 1.6 nm, reflecting a stable and compact structure (Fig. 6c).

Analysis of the solvent-accessible surface area (SASA) also showed initial fluctuations for all compounds, indicating structural adjustments before stabilization. CID-631675 had SASA values ranging from 85 to 95 nm², suggesting moderate solvent exposure. CID-9603144 displayed higher SASA values, up to 105 nm², indicating greater exposure and less compact binding. CID-91722819 fluctuated between 90 and 105 nm², reflecting significant solvent exposure. In contrast, CID-624232 exhibited the lowest SASA values, around 85 to 95 nm², indicating the most compact binding and minimal solvent exposure (Fig. 6d).

Table 6 — The pharmacokinetic properties of the active constituents of *S. italica* (Mill.)

Compounds	MW	HBD	HBA	Log P	Log S	BBB Permeability	GI Absorption	Cytotoxicity
1	334.78	2	4	1.36	-6.05	No	High	No
2	279.27	1	4	4.33	-7.06	Yes	High	No
3	283.39	1	2	5.42	-6.12	Yes	High	No
4	350.41	0	2	5.28	-8.30	Yes	High	No
5	344.41	0	3	4.47	-7.74	Yes	High	No
6	331.68	0	6	3.05	-3.73	Yes	High	No
7	336.69	1	6	0.26	-3.73	No	High	No
8	301.24	1	5	3.92	-6.68	Yes	High	No
9	231.21	0	4	-0.50	-2.67	No	High	No
10	426.38	1	7	6.53	-8.99	Yes	Low	No
11	295.65	0	5	1.79	-4.87	No	High	No
12	386.01	0	4	6.81	-7.95	No	Low	No
13	308.33	1	5	4.28	-6.35	Yes	High	No
14	312.39	1	3	3.07	-6.88	No	High	No
15	299.25	1	7	2.40	-3.06	No	High	No

MW: Molecular Weight, HBD: Hydrogen Bond Donor, HBA: Hydrogen Bond Acceptor, BBB: Blood Brain Barrier, GI: Gastrointestinal

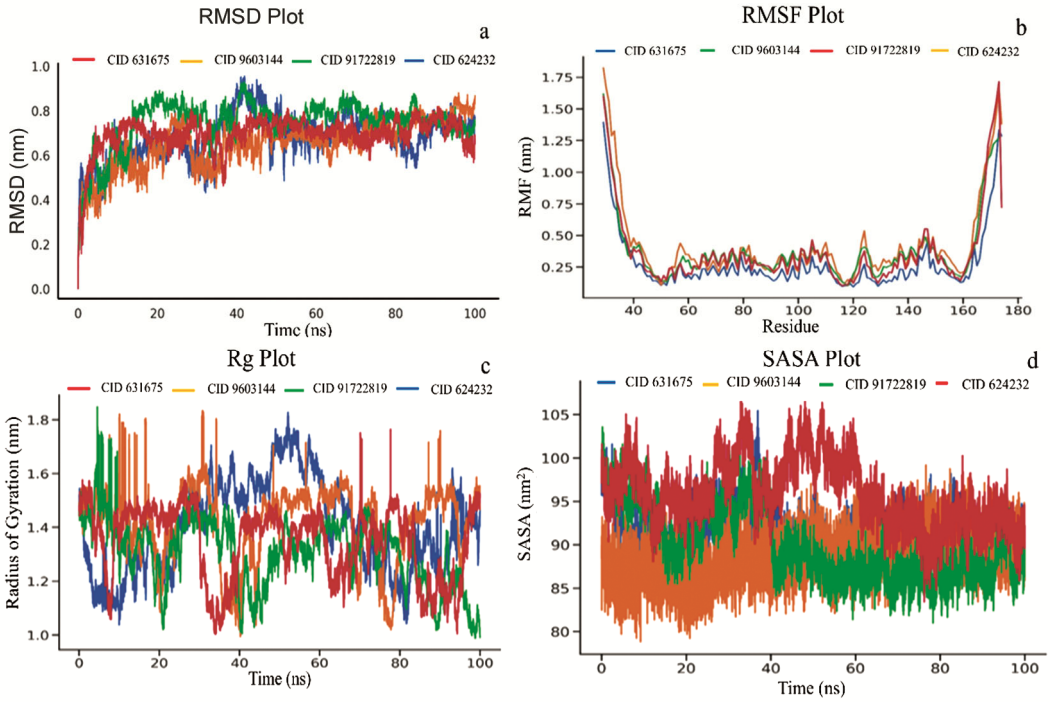

Fig. 6 — Molecular dynamics simulation analysis of the four selected compounds from *S. italica* (Mill.) in complex with caspase-3, showing: a) root mean square deviation (RMSD), b) root mean square fluctuation (RMSF), c) radius of gyration (Rg), and d) solvent-accessible surface area (SASA) plots over the simulation period.

Hydrogen bonding plays a critical role in maintaining the stability and binding affinity of protein–ligand complexes. A greater number of hydrogen bonds reflects stronger and more stable interactions. The graphical representation of the compound CID-631675 (red) shows that the least number of hydrogen bonds consistently form around 2 to 4 bonds. This suggests the interactions among the four complexes are weakest. Incompound CID-9603144 (orange), moderate hydrogen bonding frequently forms between 4 and 8 bonds, indicating stable but slightly weaker interactions compared with complex 631675. Compound CID-91722819 (green) has fewer hydrogen bonds, generally around 2 to 4 bonds, indicating weaker interactions with the protein. Meanwhile, compound CID-624232 (blue) showed a relatively high number of hydrogen bonds, frequently reaching up to 10 bonds, especially between 60 and 80 ns. This indicates strong and stable interactions with the protein (Fig. 7).

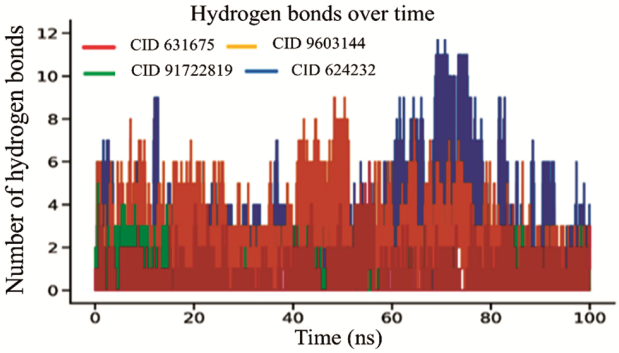

Fig. 7 — Hydrogen bond analysis of the four selected compounds from *S. italica* (Mill.) in complex with caspase-3, showing the number and stability of hydrogen bonds formed during the molecular dynamics simulation.

The figure shows the effects of four different ligands on the secondary structure of a protein during a 100 nssimulation. The CID-631675-protein complex exhibited significant structural changes over time, with the alpha-helix and extended-strand structures consistently present throughout the simulation. There were frequent transitions between the coil and turn structures, resulting in moderate fluctuations in the secondary structure and indicating moderate stability (Fig. 8a). The CID-9603144-protein complex showed more fluctuations in secondary structures, with alpha-helix and extended-strand structures being less consistent. There were more transitions to coil and

turn structures, indicating less stable binding and greater structural flexibility (Fig. 8b).

However, the CID-91722819-protein complex appeared to exhibit the most significant secondary structure fluctuations. Alpha-helix and extended-strand structures are present, but they are highly unstable, with frequent transitions to coil and turn structures, indicating high flexibility. The high degree of structural changes suggested weak binding and significant structural disruption compared with the previous protein complexes (Fig. 8c). Meanwhile, the compound CID-624232-protein complex has relatively stable secondary structures over time. The alpha-helix and extended-strand structures are consistent and fluctuate less. There are fewer transitions to coils and turns. The stability of the secondary structures indicated strong binding and minimal structural disruption (Fig. 8d).

Torsion angles provide information about ligand flexibility and conformational changes. Lower torsion angle values indicate more stable and less flexible conformations, whereas higher torsion angle values suggest increased flexibility and conformational changes. Compound CID-631675 exhibited torsion angles ranging between 80 and 120°, indicating moderate flexibility and conformational changes over time. In contrast, compound CID-9603144 demonstrated higher torsion angles, mostly between 80 and 120°, indicating more flexibility and significant conformational changes, which implies less stable binding. However, compound CID-91722819 showed the highest torsion angles, ranging between 40 and 80°, indicating considerable flexibility and frequent conformational changes, which suggests less stable binding. The compound CID-624232 displayed the lowest torsion angles ranging between 30 and 60°, indicating minimal conformational changes and the most stable and least flexible conformation among the four compounds (Fig. 9).

Molecular mechanics generalized Born surface area (MM-GBSA) analysis of the four protein-ligand

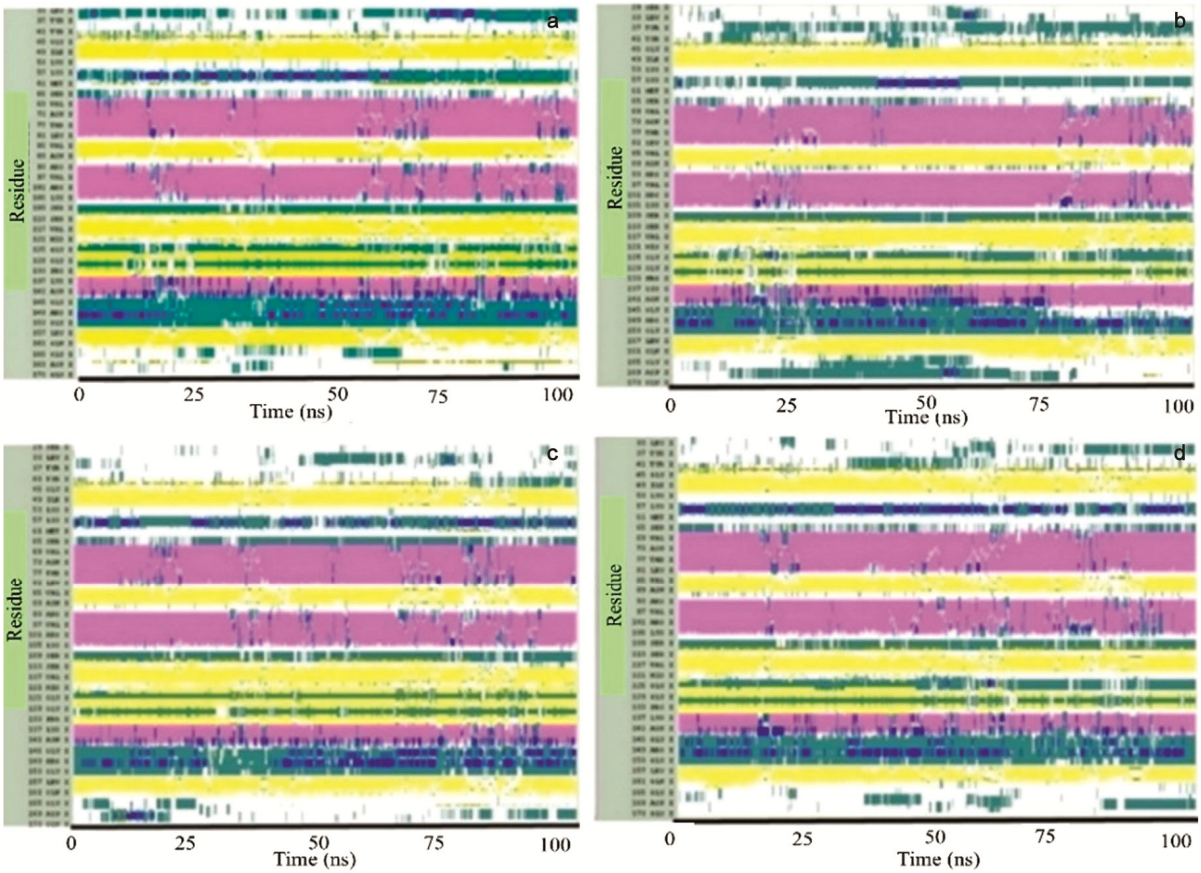

Fig. 8(a-d) — Analysis of secondary structure elements for caspase-3 in complex with four selected compounds: a) CID-631675, b) CID-9603144, c) CID-91722819, and d) CID-624232 from *S. italica* (Mill.) during molecular dynamics simulation, showing the stability and changes of α-helices, β-sheets, and other structural motifs.

complexes reveals significant differences in binding energetics and stability. In the CID-631675-protein complex, the GGAS component was highly negative, reflecting strong favourable interactions between the ligand and protein. This is complemented by a total negative energy, indicating favourable binding. The GSOLV component while positive is smaller in magnitude, further supporting the favourable interaction profile. The per-residue energetic contributions revealed several residues with strong negative values, underscoring their critical role in ligand stabilization. The negative Gibbs free energy (ΔG) highlights spontaneous and favourable binding. Both enthalpic (ΔH) and entropic (TΔS) components positively reinforce the binding stability (Fig. 10a&e). For the CID-9603144-protein complex, the GGAS component was negative but less pronounced, and the GSOLV component was positive and higher compared with other complexes, leading to a less negative total energy, indicating moderately favourable interactions. The heatmap revealed a mix of negative and positive residue contributions, suggesting moderate stabilization of the compound. The Gibbs free energy (ΔG) is positive, indicating less spontaneous and favourable binding (Fig. 10b&f).

The CID-91722819-protein compound exhibits a relatively less pronounced negative GGAS component, and a higher positive GSOLV component, resulting in less negative energy and weaker favourable interactions. The MM-GBSA heatmap shows fewer residues with strong negative contributions, suggesting less effective ligand stabilization. The Gibbs free energy (ΔG) was positive, indicating the least spontaneous and least favourable binding among the four compounds (Fig. 10c & g). In contrast, the CID-624232-protein complex exhibited a positive Gibbs free energy (ΔG), indicating that the binding was less spontaneous and less favourable. However, the positive ΔG suggests that the interactions are not as energetically favourable or spontaneous as those in the CID-631675-protein complex (Fig. 10d & h).

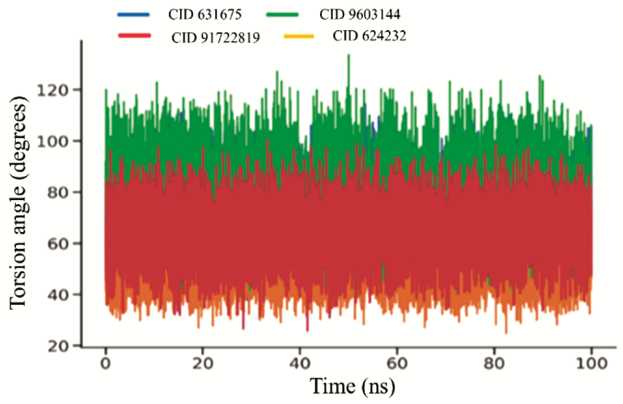

Fig. 9 — Ligand torsion angle analysis of the four selected compounds from *S. italica* (Mill.) in complex with caspase-3, showing the flexibility and conformational changes of the ligands during the molecular dynamics simulation.

Cell death analysis

The MTT assay is the first indication to assess the initial activity of novel anticancer drugs. In this study, the antiproliferative investigations showed that DOX-treated normal HSF cells displayed a significant reduction in cell viability with an IC_{50} of 1.135± 2.35 µg/mL, following 24 hours of treatment (Table 7 and Fig. 11a), compared to treated cells with *S. italica* extract that deomonstrated no toxic activities on cell growth with an IC_{50} of 869.6±5.04 µg/mL, (Table 7 and Fig. 12a). In comparison to the BC cells MDA-MB-231 treated with DOX that revealed a significant growth-inhibition with an IC_{50} of 1.27± 0.12 µg/mL (Table 7 and Fig. 13a), the experimental results showed that all cultured BC cells treated with pure ethanolic extract of *S. italica* for 24 hours and 48 hours, did not inhibit cell proliferation at lower concentrations of 50, 100, and 200 µg/mL. However, a gradual reduction in cell growth was notable between 400 and 800 µg/mL. The lowest IC_{50} concentration was observed in T47D cells (Fig. 14a), followed by MCF-7 (Fig. 15a) and MDA-MB-231 cells (Fig. 16a) with IC_{50} values of 222.03±3.25, 239.07±2.73, and 279.05±2.92 µg/mL, following 48 hours of treatment (Table 7). Meanwhile, LC HePG2 cells treated with DOX showed inhibition in cell proliferation with an IC_{50} of 16.73±3.96 µg/mL (Table 7 and Fig. 17a). In contrast, a higher significant inhibition in cell growth was demonstrated at a concentration of 200 µg/mL and continued to decrease proliferation with increasing concentrations at 400 and 800 µg/mL, with anIC_{50} value of 98.04±2.23 µg/mL following 48 hours of treatment with *S. italica* extract (Table 7 and Fig. 18a), *p-value*< 0.05 was regarded statistically significant. The *p-value*<0.001 was represented by (***) asterisk mark.

Cell morphology analysis

Morphological changes in BC and LC cancer cells were examined using inverted microscope. The untreated breast cancer cells (control cells) exhibited a phenotype resembling that of fibroblasts and were highly confluent. Microscopical examinations showed

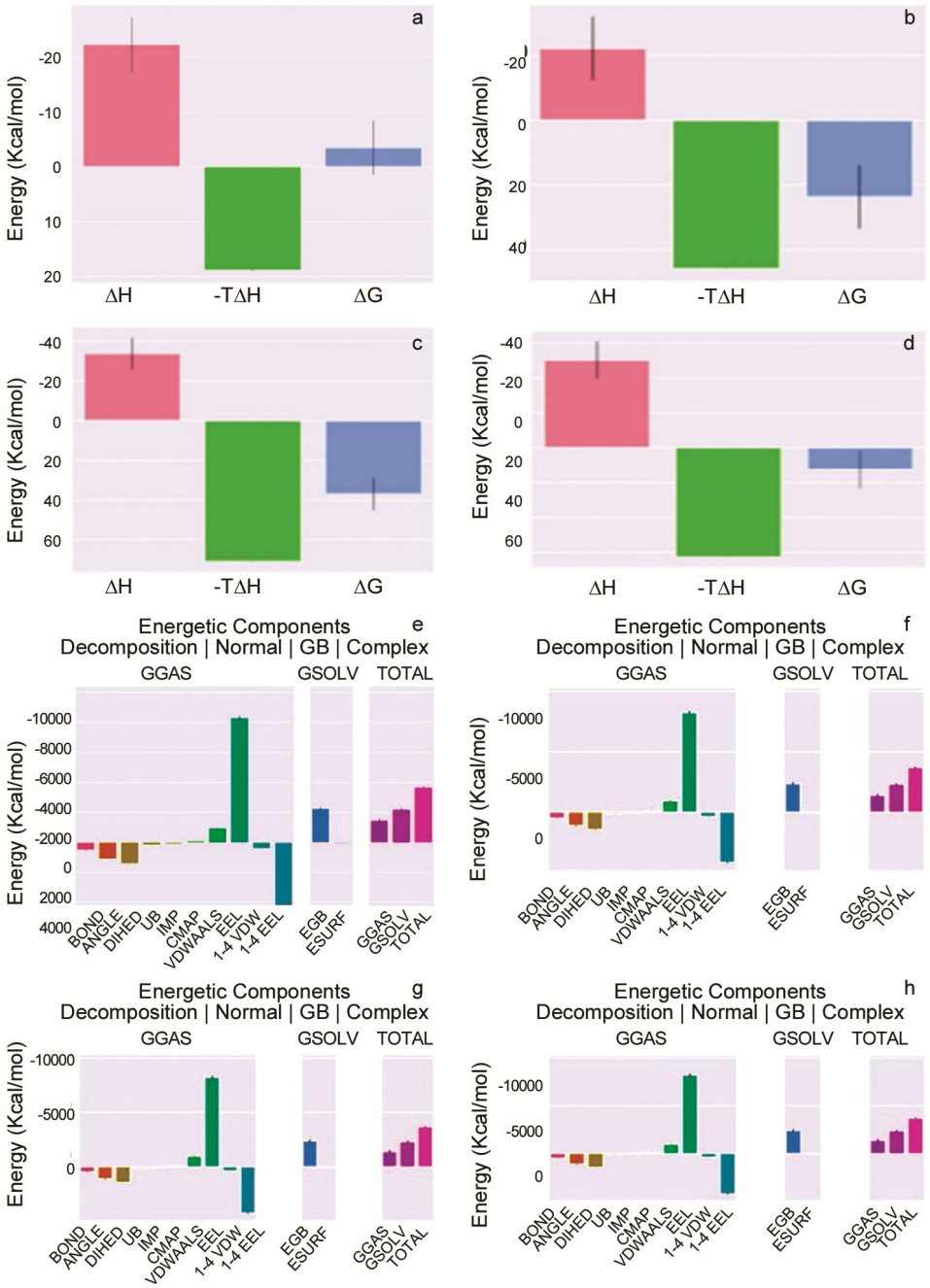

Fig. 10(a-d) — Molecular mechanics generalized Born surface area (MM-GBSA) analysis of the four selected compounds: (a&e) CID-631675, (b&f) CID-9603144, (c&g) CID-91722819, and (d&h) CID-624232 from *S. italica* (Mill.) in complex with caspase-3, showing the binding free energy contributions during the molecular dynamics simulations.

that DOX-treated HSF cells exhibited severe morphological disruptions, including cell rounding, detachment, and loss of membrane integrity (Fig. 12b), in comparison to *S. italica* extract-treated HSF cells that remained preserved, spindle-shaped with intact cell membranes and nuclei, indicating no cytotoxic effects of extracted *S. italica* components (Fig. 13b). Treatment of BC MCF-7 (Fig. 14b), T47D (Fig. 15b), and MDA-MB-231 (Fig. 16b) cells with *S. italica* extract at a concentration of 200 µg/mL showed minimal morphological changes, with most cells maintaining their tumorigenic characteristics. However, DOX-treated BC MDA-MB-231 (Fig. 13b) cells and LC

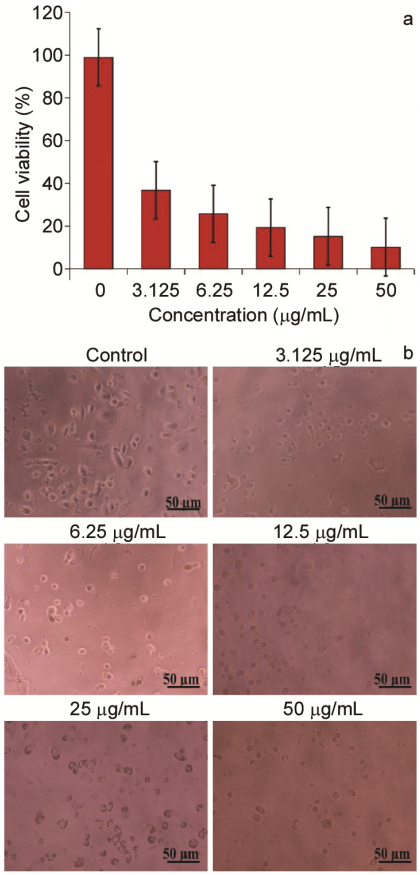

Fig. 11 — Cell death analysis of DOX-treated normal HSF cells showing: a) cell viability, and b) morphological changes at various concentrations (0–50 µg/mL) after 24 h of treatment. Images were captured using an inverted microscope (LABOMED®) at 20× magnification.

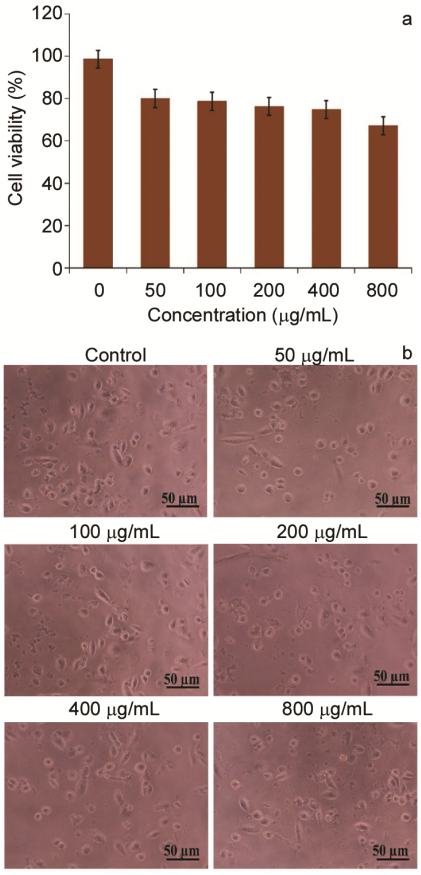

Fig. 12 — Cell death analysis of *S. italica* (Mill.) extract–treated normal HSF cells showing: a) cell viability, and b) morphological changes at various concentrations (0–800 µg/mL) after 24 h of treatment. Images were captured using an inverted microscope (LABOMED®) at 20× magnification.

Table 7 — IC_{50} values of cultured different breast and liver cancer cells treated with *S. italica* (Mill.) for 24 and 48 hours

		Experimental cell lines				
		HSF	MCF-7	T47D	MDA-MB-231	HePG2
DOX	24 h	1.135±2.35			1.27±0.12	16.73±3.96
S. italica (Mill.)	24 h	869.6±5.04	288.30±4.03	260.70±4.10	326.63±5.88	145.89±2.76
	48 h		239.07±2.73	222.03±3.25	279.05±2.92	98.04±2.23

HePG2 (Fig. 17b) cells exhibited high cytotoxic effects on the targeted cells at lower concentrations, while BC and LC cells treated with 400 µg/mL of crude extracts, a loss of spindle shape and various cellular deformations, including the formation of apoptotic bodies were observed. Moreover, the morphological changes became more apparent at a higher concentration of 800 µg/mL, with a notable reduction in the number of viable cells and an increase in detaching cells, indicating that breast cancer cells (Fig. 14b, Fig. 15b, and Fig. 16b) and liver cancer cells (Fig. 18b) were induced to undergo cell death.

SI calculations analysis

The SI values were calculated according to the applicable equation by dividing the IC_{50} value of normal HSF cells by the IC_{50} values of BC cells. The SI values were 8.87, 3.92, 3.64, and 3.12 for cancer HePGG2, T47D, MCF-7, and MDA-MB-231 cells respectively. Highly significant differences was obsereved in the LC cell line HePG2 as summarized in Table 8.

Caspase-3 activity analysis

The dose-dependent increase in the activity of caspase-3 was determined. CASPASE-Glo luminometric analysis of these proteins revealed a highly significant increase (< 0.001) in the level of the

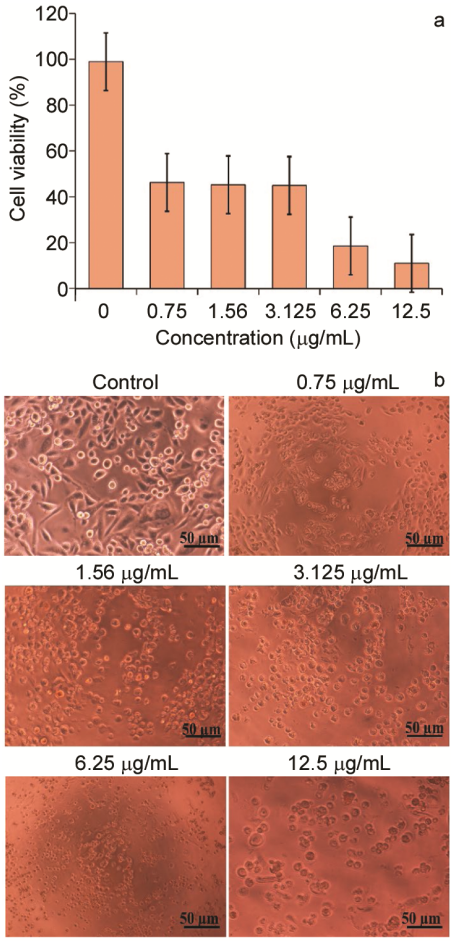

Fig. 13 — Cell death analysis of DOX-treated breast cancer MDA-MB-231 cells showing: a) cell viability, and b) morphological changes at various concentrations (0–50 μg/mL) after 24 h of treatment. Images were captured using an inverted microscope (LABOMED®) at 20× magnification.

enzymes in the treated LC HePG2 cells (of interest) with DOX and *S. italica*, respectively (Fig. 19).

Discussion

The intensity of peaks in UV-VIS and FT-IR spectra provide crucial information about the chemical composition of the materials. Samples with higher peak intensities exhibited stronger infrared absorption at specific frequencies, which correlated with the presence and concentration of certain functional groups[18]. However, the phytochemical profiling of *S. italica* extract via tri-spectroscopical UV-VIS, FT-IR, and GC-MS analysis revealed a diverse range of functional groups and secondary metabolites, which significantly correlate with the observed biological activities. The UV-VIS spectra indicated absorbance regions consistent with C=O and O=C-OH electronic transitions, associated with conjugated aromatic systems and carbonyl groups structures commonly found in bioactive phenolic and flavonoid compounds. The FT-IR data confirmed the presence of functional groups such as hydroxyl (–OH), carbonyl (C=O), olefinic (C=C), and glycosidic bonds, all of which are critical in modulating oxidative stress and interacting with cellular targets, potentially leading to apoptosis in cancer cells, suggesting the important role of phenolics that possess antioxidant and antiproliferative activities through the regulation of oxidative stress[19]. These compounds vary in complexity from basic phenolic molecules to highly polymerized compounds and can

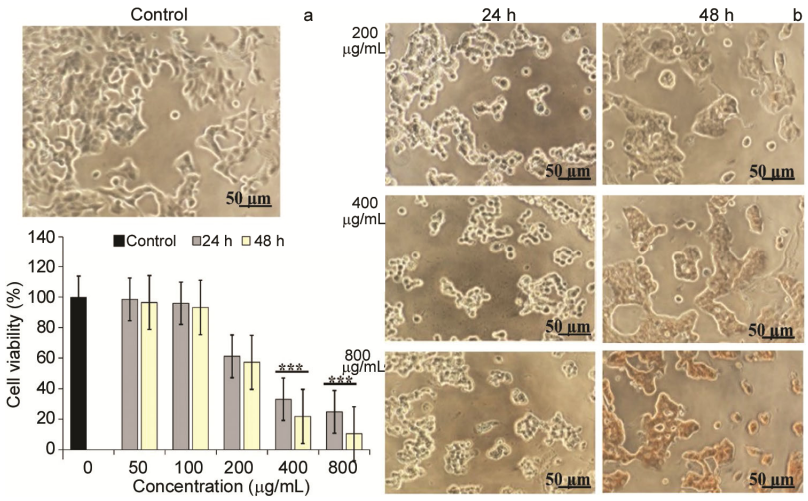

Fig. 14 — Cell death analysis of *S. italica* (Mill.) extract–treated breast cancer MCF-7 cells showing: a) cell viability, and b) morphological changes at various concentrations (0–800 μg/mL) after 24 h and 48 h of treatment. Images were captured using an inverted microscope (LABOMED®) at 20× magnification.

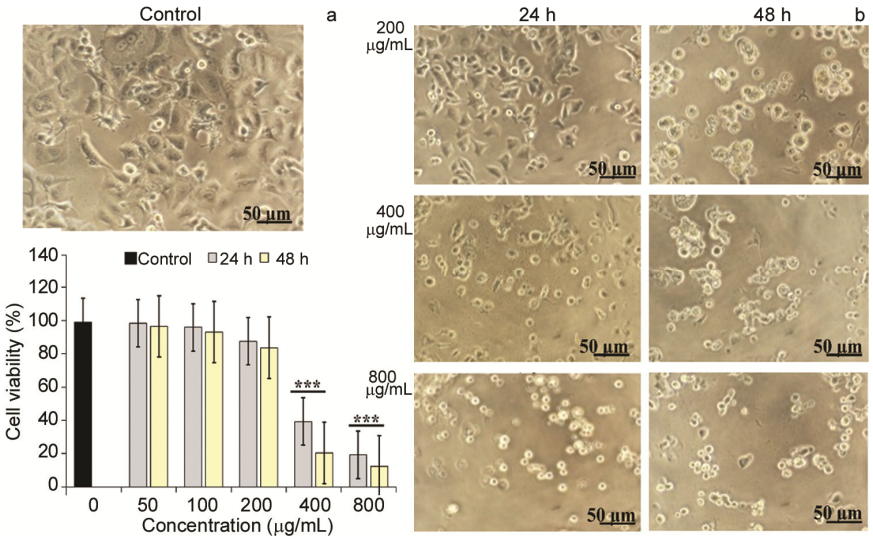

Fig. 15 — Cell death analysis of *S. italica* (Mill.) extract–treated breast cancer T47D cells showing: a) cell viability, and b) morphological changes at various concentrations (0–800 µg/mL) after 24 h and 48 h of treatment. Images were captured using an inverted microscope (LABOMED®) at 20× magnification.

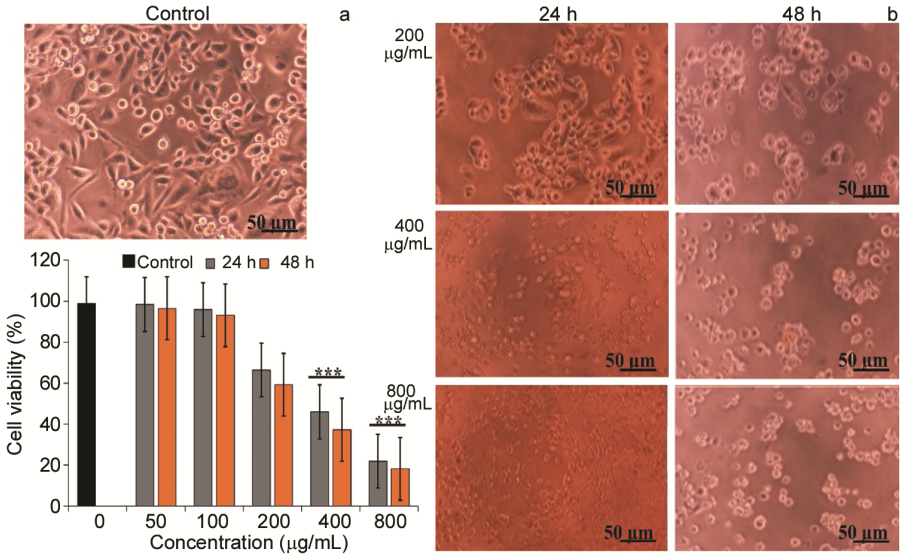

Fig. 16 — Cell death analysis of *S. italica* (Mill.) extract–treated breast cancer MDA-MB-231 cells showing: a) cell viability, and b) morphological changes at various concentrations (0–800 µg/mL) after 24 h and 48 h of treatment. Images were captured using an inverted microscope (LABOMED®) at 20× magnification.

be identified by benzene rings with one or more hydroxyl groups[20], exhibiting significant biological roles as antibacterial, antioxidant, and anti-inflammatory candidates[21].

These spectroscopic findings were substantiated by GC-MS analysis, which is the most effective method for identifying bioactive molecules of long-chain hydrocarbons, fatty acids, esters, steroids, and nitro compounds[22]. Moreover, 15 bioactive compounds were identified using gas chromatography technique, several of which belong to structural classes known for cytotoxic, anti-proliferative, and enzyme-inhibiting properties. Herein in our study, the GC-MS profile of the *S. italica* extract was characterized by the presence of novel organic compounds such as quinazoline, an organic aromatic heterocyclic compound, significantly inhibits cell cycle progression and division by downregulating protein kinases[23]. Another organic compound, phenylpyrazole, has shown promising results as an anticancer agent by inducing apoptotic and autophagic cell death pathways[24]. Benzene sulfonamide-amino, an aromatic compound,

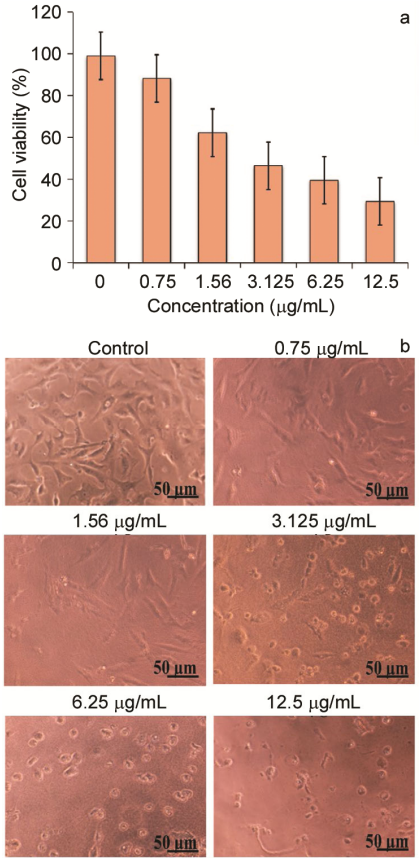

Fig. 17 — Cell death analysis of DOX-treated liver cancer HePG2 cells showing: a) cell viability, and b) morphological changes at various concentrations (0–50 µg/mL) after 24 h of treatment. Images were captured using an inverted microscope (LABOMED®) at 20× magnification.

has potent anticancer effects against both positive and negative estrogen receptors in BC cells[25]. The benzo-pyrimidin-phenyl-amin combination showed potent activities against breast, myeloid leukemia, pancreatic, and liver cancers by downregulating protein kinase C[26].

Furthermore, the selected compounds from *S. italica* were subjected to preliminary evaluation using advanced CADD tools to predict their potential therapeutic effectiveness. Among the critical parameters of Lipinski's rule of five, HBD contribute to molecular acidity, while HBA influence basicity. All four selected compounds exhibited HBD values within the ideal range, consistent with drug-like properties[27]. These results are in agreement with previous studies[28,29], which demonstrated that both hydrogen bonding and hydrophobic interactions play a crucial role in stabilizing ligands at active target sites, thereby influencing binding affinity and overall drug efficacy. Another fundamental factor is HBA, and low oral bioavailability can result from low solubility and permeability of molecules[30]. By interleaving HBA, as presented in *S. italica* compounds 10 and 12, the aqueous solubility of molecules could be optimized, thereby improving the bioavailability of the compounds[31].

Also, physicochemical properties, such as MW and lipophilicity, have been shown in recent studies to improve compound safety, efficacy, and produce positive therapeutic effects[32]. In this study, we found

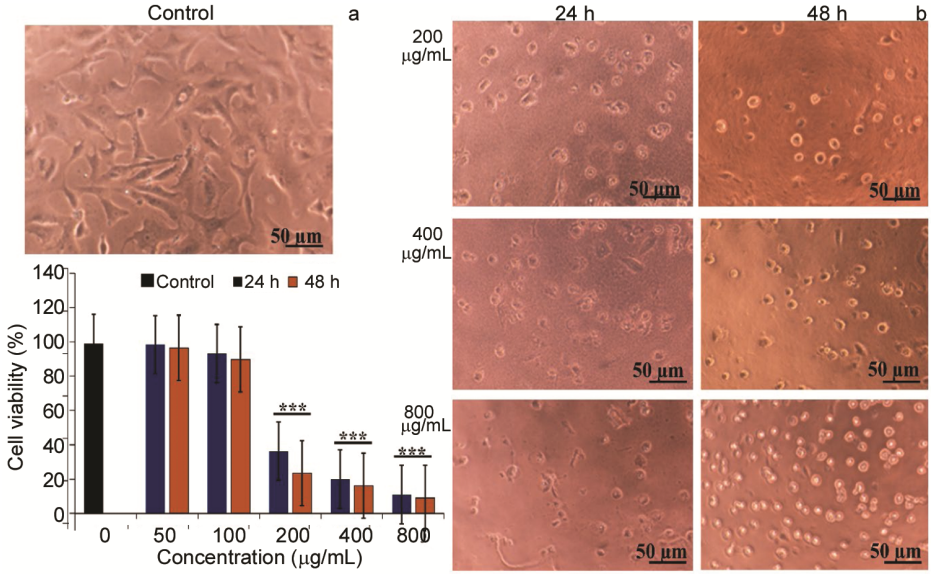

Fig. 18 — Cell death analysis of *S. italica* (Mill.) extract–treated liver cancer HePG2 cells showing: a) cell viability, and b) morphological changes at various concentrations (0–800 µg/mL) after 24 h and 48 h of treatment. Images were captured using an inverted microscope (LABOMED®) at 20× magnification.

Table 8 — SI values of ethanolic extract of *S. italica* (Mill.)

	Experimental cancer cell lines				
	MCF-7	T47D	MDA-MB-231	HePG2	Recommended range
SI values	3.64	3.92	3.12	8.87	1.96-51.3 [16]

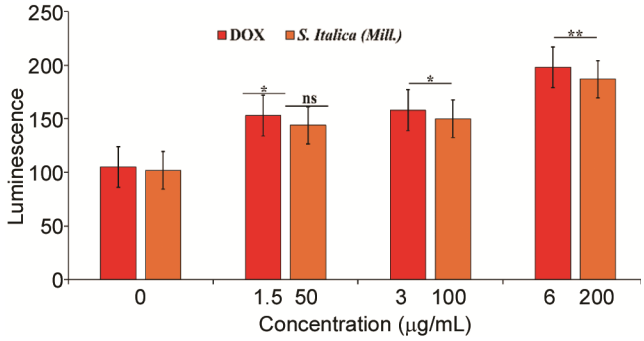

Fig. 19 — Caspase-3 activity in liver cancer HepG2 cells after 4 h of treatment with DOX and *S. italica* (Mill.) at various concentrations, measured using a luminescence microplate reader. Statistical significance was defined as $p < 0.05$ (*) *and* $p < 0.001$ (**); $p > 0.05$ was considered non-significant (ns).

that all compounds detected in *S. italica* followed Lipinski's rule, except for Log-S. Approximately 50% of the phytochemical constituents of *S. italica* exhibited poor solubility (>-6.5). The characteristic constitutional hydrophobicity may affect the solubility, and subsequently, the permeability of these bioactive compounds to cross the cell membranes of targeted cells to act efficiently. Limited solubility can significantly reduce dissolution in physiological fluids, leading to low absorption, poor systemic bioavailability, and insufficient accumulation of the drug at the tumour site. As a result, even compounds with potent *in vitro* cytotoxic activity may exhibit weak or inconsistent *in vivo* efficacy.[33].

There have been numerous studies covering the significant biological activities of *S. italica* against various microorganisms. Recently, caspase-3 attracted much attention in the field of medical research because of its critical role in tissue differentiation, regeneration, and cell apoptosis. In this study, we investigated the cytotoxic activity of *S. italica* bioactive compounds targeted a pro-apoptotic protein, caspase-3 to expand our knowledge and fill any gaps related to its significance applications as potential drug candidates.To accomplish this, docking simulations were performed using DiffDock software to identify the interactions between the caspase-3 receptor and four selected compounds from *S. italica*. This process involved generating multiple binding poses for each compound to the receptor. Each pose was evaluated based on its binding energy with the aim of identifying the most favorable ligand-receptor interaction. The compound with the lowest energy score was selected as the best candidate for further analysis, ensuring that the compound exhibited the most stable and energetically favourable binding conformation during simulation process.

Importantly, the docking results demonstrated that four compounds CID-631675, CID-9603144, CID-91722819, and CID-624232 exhibited strong binding affinities to the 1GFW receptor (a modeled cancer target), with CID-624232 showing the most stable interactions and minimal structural perturbation in molecular dynamics simulations. The chemical nature of these compounds, as revealed by FT-IR and GC-MS, supports their ability to form stable hydrogen bonds and hydrophobic interactions with key amino acid residues in the active site. These findings were similarly observed by Aboud *et al.*[34] who found that extracted compounds from *C. ternatea* flowers in metastatic breast estrogen-dependent cancer cells exhibited variable molecular and dynamic values when targeted a proapoptotic protein caspase-3.

This link between structure and function is further validated by cytotoxicity assay, where the *S. italica* extract exhibited dose-dependent growth inhibition in BC (T47D, MCF-7, MDA-MB-231) and LC (HePG2) cells, with minimal toxicity to normal HSF cells, while a higher significant activity against HCC (HePG2) cells, followed by breast ductal carcinoma (T47D), adenocarcinoma (MCF-7), and metastatic triple-negative breast cancer (MDA-MB-231) cells. These results correlate with Towanou *et al.*[35] findings, which proved that active compounds of *S. italica* have no toxic effects on vital organs, and Khalaf *et al.*[36], who found that various *S. italica* species extracts have moderate effects on the breast (MCF-7) and liver (HePG2) cancer cells. These findings may be attributed to the variability in gene expression within cells of the same tumour, contributing to cellular heterogeneity that may cause some cells to respond poorly to drug treatment[37].

In cancer research, apoptosis is one of the most crucial factors broadly studied because of its significance in and complexity in tumor regression.

Caspases play critical roles in promoting apoptosis and the development of cellular morphology involved in programmed cell death[38]. Correspondingly, caspase-3 in carcinomic cells, is closely associated with the expression of apoptosis-associated proteins and poor prognosis[39]. Natural products have consistently been shown to be valuable and abundant source of treatments for a wide range of human illnesses, including cancer[40]. The selective cytotoxicity corresponds well with the structural features observed in the phytochemical analysis, particularly the presence of polar groups facilitating membrane penetration and interaction with intracellular targets. Moreover, the increase in caspase-3 activity and observed apoptotic morphology at higher extract concentrations confirms that the active compounds likely exert their effects through apoptosis induction, a mechanism supported by both the docking and MD simulation data.

We suggest that poor solubility not only affects pharmacokinetics but also hinders drug–target interactions by limiting therapeutic concentrations within the tumour microenvironment. Hydrophobic compounds, such as those extracted from *S. italica*, often exhibit strong plasma protein binding, which further reduces their activity. In addition, precipitation during formulation or in physiological conditions can compromise both stability and delivery efficiency. Addressing solubility limitations is therefore essential for maximizing anticancer potential. Advanced formulation strategies are needed to enhance solubilization, improve bioavailability, and enable targeted delivery of hydrophobic anticancer agents, thereby increasing drug concentrations at tumor sites and improving therapeutic outcomes.

Conclusion

The integrated spectroscopic, chromatographic, and computational analyses of *S. italica* (Mill.) extract revealed a diverse array of bioactive compounds with significant anticancer potential. UV-VIS, FT-IR, and GC-MS profiling confirmed the presence of key functional groupssuch as hydroxyl, carbonyl, and aromatic rings associated with phenolic, flavonoid, and heterocyclic structures known for their antioxidant and cytotoxic properties. Computational docking and molecular dynamics simulations demonstrated strong binding affinities of selected compounds to caspase-3, particularly CID-624232(benzo-pyrimidin-fluoro-phenyl-amine), supporting their potential to induce apoptosis. *In vitro* cytotoxicity assays validated these findings by showing dose-dependent inhibition of breast and liver cancer cells with minimal effects on normal cells. Overall, the structure–activity relationship analysis provides strong evidence that *S. italica* contains promising lead compounds for anticancer drug development, acting primarily through oxidative stress modulation and caspase-mediated apoptotic pathways. Further studies are strongly recommended to enhance the solubility of the extracted compounds using an appropriate nanodelivery system, as well as to evaluate their efficacy and safety in *in vivo* models.

Acknowledgment

The authors acknowledge the technical and financial support provided by the Deanship of Scientific Research (DSR), King Abdulaziz University, Jeddah, Saudi Arabia, under grant no. (GPIP-480-130-2024).

Conflict of interest

The authors declare that they have no conflict of interest.

References

1 Sung H, Ferlay J, Siegel R L, Laversanne M, Soerjomataram I, *et al.*, Global cancer statistics 2020: GLOBOCAN estimates of incidence and mortality worldwide for 36 cancers in 185 countries, *CA Cancer J Clin*, 2021, **71**, 209- 249, doi: 10.3322/caac.21660.

2 Arnold M, Morgan E, Rumgay H, Mafra A, Singh D, *et al.*, Current and future burden of breast cancer: Global statistics for 2020 and 2040, *Breast*, 2022, **66**, 15-23, doi: 10.1016/j.breast.2022.08.010.

3 Chen J G, Zhu J, Zhang Y H, Chen Y S, Lu J H, *et al.*, Liver cancer mortality over six decades in an epidemic area: What we have learned, *Peer J*, 2021, **9**, e10600, doi: 10.7717/peerj.10600.

4 Zhu Y, Xie N, Chai Y, Nie Y, Liu K, *et al.*, Apoptosis induction, a sharp edge of berberine to exert anti-cancer effects, focus on breast, lung, and liver cancer, *Front Pharmacol*, 2022, **13**, 803717, doi: 10.3389/ fphar.2022.803717.

5 Ullah R, Alqahtani S, Noman M, Alqahtani M, Ibenmoussa S, *et al.*, A review on ethno-medicinal plants used in traditional medicine in the Kingdom of Saudi Arabia, *Saudi J Biol Sci*, 2020, **27**(10), 2706-2718, doi: 10.1016/ j.sjbs.2020.06.020.

6 Azani N, Babineau M, Bailey D, Banks H, Barbosa R, *et al.*, A new subfamily classification of the Leguminosae based on a taxonomically comprehensive phylogeny: The Legume Phylogeny Working Group (LPWG), *Taxon*, 2017, **66**(1), 44-77.

7 Marazzi B, Endress P K, Queiroz LP and Conti E, Phylogenetic relationships within Senna (Leguminosae,

Cassiinae) based on three chloroplast DNA regions: patterns in the evolution of floral symmetry and extra floral nectaries, *Am J Bot*, 2006, **93**(2), 288-303, doi: 10.3732/ajb.93.2.288.

8 Adjou S, Koudoro Y, Nonviho G, Ahoussi D and Sohounhloue C, Phytochemical profile and potential pharmacological properties of leaves extract of *Senna italica* Mill, *Am J Pharm Sci*, 2021, **9**(1), 36-39.

9 Dike S, Emejulu A, Chukwudoruo S, Akpaki A, Nsofor N, *et al.*, GC-MS and FTIR analyses of bioactive compounds present in ethanol leaf extract of Sidaacuta from Imo State, Nigeri, *GSC Biol Pharm Sci*, 2013, **25**(2), 394-404.

10 Pawar S and Rohane H, Review on discovery studio: An important tool for molecular docking, 2021.

11 Jin W, Yang Q, Huang B, Bao Z, Su B, *et al.*, Enhanced solubilization and extraction of hydrophobic bioactive compounds using water/ionic liquid mixtures, *Green Chem*, 2016, **18**(12), 3549-3557.

12 Menaga S, Jayanthi G and Haritha P, Phytochemical and antimicrobial screening of *Senna italica* Mill. Leaf, *Scie Xplore: Inter J Res Sci*, 2020, 30-35.

13 Zibaee E, Javadi B, Sobhani Z, Akaberi M, Farhadi F, *et al.*, Cassia species: A review of traditional uses, phytochemistry and pharmacology, *Pharmcol Res-Mod Chin Med*, 2023, 100325.

14 Alharbi T A, Alzahrani D A and Alfarhan A H, Floristic diversity and vegetation analysis of Radwa Mountain, Al-Madinah Region, Saudi Arabia, *Saudi J Biol Sci*, 2022, **29**(4), 2992–3003, doi: 10.1016/j.sjbs.2022.01.035.

15 Abraham J, Murtola T, Schulz R, Páll S, Smith C, *et al.*, GROMACS: High performance molecular simulations through multi-level parallelism from laptops to supercomputers, *Software X*, 2015, **1**, 19-25.

16 Indrayanto G, Putra G S and Suhud F, Validation of *in-vitro* bioassay methods: Application in herbal drug research, *Profiles Drug Subst Excip Relat Methodol*, 2021, **46**, 273-307, doi: 10.1016/bs.podrm.2020.07.005.

17 Lipinski C A, Lombardo F, Dominy B W and Feeney P J, Experimental and computational approaches to estimate solubility and permeability in drug discovery and development settings, *Adv Drug Deliv Rev*, 2019, **101**, 23–43, doi: 10.1016/j.addr.2019.01.001.

18 AL-Kadhemy H and Alwaan M, FTIR spectrum of laser dye fluorescein doped polymer PMMA films, *Res Rev Polym*, 2012, **3**(3), 102-106.

19 Lin D, Xiao M, Zhao J, Li Z, Xing B, *et al.*, An overview of plant phenolic compounds and their importance in human nutrition and management of Type 2 diabetes, *Molecules*, 2016, **21**(10), 1374, doi: 10.3390/molecules21101374.

20 Verma R, Akanksha K, Jha K and Rani L, Comparative studies of functional groups present in invasive and economically important plant leaf methanolic extracts by using FTIR spectroscopic analysis, *GSC Biol Pharm Sci*, 2023, **23**(3), 184-191.

21 Albuquerque B R, Heleno S A, Oliveira M B P P, Barros L and Ferreira I C F R, Phenolic compounds: Current industrial applications, limitations and future challenges, *Food Funct*, 2021, **12**(1), 14-29.

22 Karuppasamy B, Nishanthini A and Mohan V R, GC-MS analysis of *Polycarpaea corymbosa* (L.) Lam whole plant, *Asian Pac J Trop Biomed*, 2012, **2**(3), 1289-1292.

23 Karamouzis M V, Grandis J R and Argiris A, Therapies directed against epidermal growth factor receptor in aerodigestive carcinomas, *JAMA*, 2007, **298**(1), 70-82.

24 Leong S W, Wang J, Okuda K S, Su Q, Zhang Y, *et al.*, Discovery of a novel dual functional phenylpyrazole-styryl hybrid that induces apoptotic and autophagic cell death in bladder cancer cells, *Eur J Med Chem*, 2023, **254**, 115335.

25 Mohamed H S, Abdelgawad M A, Hegab M, Hamza Z S, Nagdy A M, *et al.*, Computational and molecular docking studies of new benzene sulfonamide drugs with anticancer and antioxidant effects, *Curr Org Synth*, 2023, **20**(3), 339-350.

26 Stanetty P, Hattinger G, Schnürch M and Mihovilovic M D, Novel and efficient access to phenylamino-pyrimidine type protein kinase C inhibitors utilizing a Negishi cross-coupling strategy, *J Org Chem*, 2005, **70**(13), 5215-5220.

27 Sliwoski G, Kothiwale S, Meiler J and Lowe Jr, Computational methods in drug discovery, *Pharm Rev*, 2013, **66**(1), 334-95, doi: 10.1124/pr.112.007336.

28 Patil S, Rane B, Shinde S and Deokar S, *In silico* pharmacokinetic and drug-likeness evaluation of bioactive natural compounds: Application of Lipinski's rule of five, *J Biomol Struct Dyn*, 2022, **40**(15), 6593–6605, doi: 10.1080/07391102.2021.1923850.

29 Patil R, Das S, Stanley A, Yadav L, Sudhakar A, *et al.*, Optimized hydrophobic interactions and hydrogen bonding at the target-ligand interface leads the pathways of drug-designing, *PLoS One*, 2010, **5**(8), e1202, doi: 10.1371/journal.pone.0012029.

30 Savjani K T, Gajjar A K and Savjani J K, Drug solubility: Importance and enhancement techniques, *Int Sch Res Not*, 2012, **2012**(1), 95727, doi: 10.5402/2012/195727.

31 Sharom F J, ABC multidrug transporters: structure, function and role in chemoresistance, *Pharmacogenomics*, 2008, **9**(1), 105-127, doi: 10.2217/14622416.9.1.105.

32 Arnott J A and Planey S L, The influence of lipophilicity in drug discovery and design, *Expert Opin Drug Discov*, 2012, **7**(10), 863-875, doi: 10.1517/17460441. 2012. 714363.

33 Loftsson T and Brewster M E, Pharmaceutical applications of cyclodextrins: Basic science and product development, *J Pharm Pharmacol*, 2022, **74**(8), 1027–1049, doi: 10.1093/jpp/rgac042.

34 Aboud F, Al-Shaeri M, Zari A, Ali E and Almalki N, Molecular docking and dynamic simulation of phytochemical components from *Clitoria ternatea* against different hormone-dependent cancer cell lines, *Ind J Chem*, 2025, **64**(2), 192-212, doi: 10.56042/ijc.v64i2.15354.

35 Towanou R, Konmy B, Yovo M, Dansou C C, Dougnon V, *et al.*, Baba-Moussa L. phytochemical screening, antioxidant activity, and acute toxicity evaluation of *Senna italica* extract used in traditional medicine, *J Toxicol*, 2023, **2023**, 6405415, doi: 10.1155/2023/6405415.

36 Khalaf M, Ghareeb A, Saad M, Madkour M, El-Ziaty K, *et al.*, Phenolic constituents, antimicrobial, antioxidant, and anticancer activities of ethyl acetate and n-butanol extracts of *Senna italica*, *Acta Chromatographica*, 2019, **31**(2), 138-145.

37 Liu K, Newbury P A, Glicksberg B S, Zeng W Z D, Paithankar S, *et al.*, Evaluating cell lines as models for

metastatic breast cancer through integrative analysis of genomic data, *Nat Commun*, 2019, **10**(1), 2138, doi: 10.1038/s41467-019-10148-6.

38 Bratton S B, MacFarlane M, Cain K and Cohen G M, Protein complexes activate distinct caspase cascades in death receptor and stress-induced apoptosis, *Exp Cell Res*, 2000, **256**(1), 27-33, doi: 10.1006/excr. 2000.4835.

39 Yang X H, Sladek T L, Liu X, Butler B R, Froelich C J, *et al.*, Reconstitution of caspase 3 sensitizes MCF-7 breast cancer cells to doxorubicin- and etoposide-induced apoptosis, *Cancer Res*, 2001, **61**(1), 348-354.

40 Atanasov G, Zotchev B, Dirsch M and Supuran T, Natural products in drug discovery: Advances and opportunities, *Nat Rev Drug Discov*, 2021, **20**(3), 200-216, doi: 10.1038/s41573-020-00114-z.